JOURNAL OF SOLID STATE CHEMISTRY **128,** 80–86 (1997)
ARTICLE NO. SC967158

Stoichiometry of Li_2MnO_3 and $LiMn_2O_4$ Coexisting Phases: XRD and EPR Characterization

V. Massarotti, D. Capsoni, and M. Bini

Dipartimento di Chimica Fisica and CSTE-CNR, Universita' degli Studi di Pavia, via Taramelli 16, I-27100 Pavia, Italia

C. B. Azzoni

Istituto Nazionale di Fisica della Materia, Dipartimento di Fisica ''Alessandro Volta,'' Universita' degli Studi di Pavia, via Bassi 6, I-27100 Pavia, Italia

and

A. Paleari

Istituto Nazionale di Fisica della Materia, Dipartimento di Fisica, Universita' degli Studi di Milano, via Celoria 16, I-20133 Milan, Italia

Received May 13, 1996; in revised form September 13, 1996; accepted September 17, 1996

The coexistence of $LiMn_2O_4$ and Li_2MnO_3 phases from MnO/Li_2CO_3 mixtures with lithium cationic fraction $0.33 \leq x \leq 0.53$ was studied by X-ray diffraction (XRD) and electron paramagnetic resonance (EPR) measurements. XRD quantitative phase analysis was carried out using the Rietveld profile refinement procedure, while the Li_2MnO_3 percentage was determined directly by comparing the EPR intensities with the intensity of the pure Li_2MnO_3 spectrum. The experimental results show the presence of an Li-rich spinel phase and allow an estimation of the lithium excess, since the structural analysis of pure Li_2MnO_3 samples evidenced a nearly stoichiometric composition ($x = 0.663$) with very limited cationic disorder. © 1997 Academic Press

1. INTRODUCTION

Li–Mn–O compounds have recently received growing interest in both theoretical and applicative fields since the $LiMn_2O_4$ spinel and related phases possess peculiar properties suited for applications in the fields of electrochemistry (1–4) and catalysis (5–7) and in lithium ion selective detectors (8).

In a previous work (9) the formation of $LiMn_2O_4$ from the reactive system MnO/Li_2CO_3 was studied by X-ray diffraction (XRD) measurements. The presence of Mn_3O_4 and Li_2MnO_3 phases, in addition to the spinel, was evidenced in samples with starting lithium cationic fraction $x < 0.33$ and $x > 0.35$, respectively. Also, for $x > 0.35$, a nonstoichiometric spinel phase was also observed. XRD patterns on samples with $0.33 < x < 0.35$ showed the stoichiometric phase only, whose cubic lattice parameter had, however, a marked x dependence. The same feature was observed for $x > 0.35$, suggesting the existence of point defects involving Li^+ ions.

In order to assess the spinel stoichiometry, more details on the structure of the coexisting Li_2MnO_3 are needed for the quantitative determination of the phases. It was reported that a significant Li–Mn disorder (about 12%) occurs in Li_2MnO_3 samples obtained by solid state reaction (10). Such cationic disorder should be relevant in the cation layers (Mn_2Li) whose stacking is ruled by the presence of a mirror plane parallel to the *ac* plane, in contrast to the Li_2SnO_3 case. The coordination octahedra are distorted because of the different sizes of Li^+ and Mn^{4+} ions. Each oxygen octahedron around the Mn^{4+} ion (four in the unit cell) shares the edges with 12 neighboring octahedra, three of which center on other Mn^{4+} ions. The distortion is also due to the strong repulsion between nearest neighbors Mn^{4+} ions, minimized by Mn–O–Mn angles larger than 90° (about 96°, in this case). On the other hand, smaller O–Mn–O angles (down to 84°) occur for oxygens constituting edges shared with neighboring MnO_6 octahedra.

To identify distinct lithium and manganese sites in the spinel-type oxides ($LiMn_2O_4$, Mn_3O_4) and rock salt-type (Li_2MnO_3) other methods more sensitive than the XRD are required. In this direction, the identification of distinct Li sites in $LiMn_2O_4$ and Li_2MnO_3 has been recently obtained by ^6Li and ^7Li nuclear magnetic resonance (NMR) spectroscopy (8).

The aim of our work was the assessment of the structures of coexisting $LiMn_2O_4$ and Li_2MnO_3 phases, taking into

0022-4596/97 $25.00

account the cationic order and lithium overstoichiometry. In order to quantify the amount of the two phases, allowing a reliable determination of lithium excess, electron paramagnetic resonance (EPR) data from samples previously characterized by XRD were analyzed. The results confirm the existence of a Li-rich spinel phase and show that in Li_2MnO_3 the cationic disorder is indeed more limited than previously supposed.

2. EXPERIMENTAL DETAILS

2.1. Materials and Sample Preparation

Samples were prepared by the reactive system Alfa (99.9%) MnO/Carlo Erba (R.P.) Li_2CO_3 from a starting mixture with $0.33 \leq x \leq 0.53$. Each mixture was fired 8 h in air at 800°C and 8 h at 900°C. Both heating and cooling rates were 5°C/min. Pure Li_2MnO_3 was obtained from the reactive mixture with $x = 0.667$ following the thermal treatment just described.

2.2. Apparatus and Procedures

Diffraction data were obtained using a Philips PW1710 powder diffractometer equipped with a Philips PW1050 vertical goniometer (Cu$K\alpha$ radiation ($K\alpha_1 = 1.54056$ Å, $K\alpha_2 = 1.5443$ Å) with a graphite monochromator). Patterns were collected in the angular range $15^\circ < 2\theta < 130^\circ$ in steps of 0.02° with 10 s of counting time.

Structural and profile parameters were obtained by the Rietveld refinement procedure (11) performed with the WYRIET Version 3.5 (12) and DBWS (13) programs. More detailed description about Rietveld refinement of multiphase system was reported in previous papers (9, 14). The relative phase amounts were obtained by the procedure of Hill and Howard (15) and corrected for microabsorption effects. In order to fit the observed patterns the presence of the following compounds was considered:

(i) $LiMn_2O_4$—spinel type ($x = 0.33$), space group $Fd3m$, $a \cong 8.241$ Å: atomic positions, with respect to the origin at the center, deduced from Ref. (16); 35 Bragg reflections.

(ii) Li_2MnO_3 ($C2/m$): monoclinic, $a \cong 4.924$ Å, $b \cong 8.522$ Å, $c \cong 5.024$ Å, $\beta \cong 109.4^\circ$: atomic positions according to (10); 198 Bragg reflections.

The profile coefficients of a Pearson VII function were refined (12, 13). Structural and profile parameters were determined for pure Li_2MnO_3 ($x = 0.667$), as well as its stoichiometry from the occupancy factors. However, when a low percentage of Li_2MnO_3 coexisted with the spinel phase, only the scale factor, lattice constants, and profile parameters were refined. Owing to the poor scattering power of Li^+ ions, it is very difficult to obtain reliable values of the pertinent occupancy factor or the stoichiometry of the compound.

EPR measurements were carried out using a Bruker spectrometer in the X band (about 9.12 GHz) in the temperature range 120–300 K. The concentration of EPR centers was estimated by comparing the signal areas with that of pure Li_2MnO_3 and taking particular care as to the reproducibility of the sample position in the resonant cavity. The shape and area of the EPR spectra were analyzed by numerical methods.

3. RESULTS

3.1. XRD Analysis

The investigated samples in the composition range $0.33 < x < 0.53$ were characterized by XRD patterns dominated by the lines expected from the spinel phase (Fig. 1). In samples with $x > 0.35$ the reflections of the Li_2MnO_3 phase become detectable and their intensities increase with x. During the structural parameter refinement, care was taken to reach the best agreement between calculated and observed diffraction intensities for the Li_2MnO_3 phase, especially when it constituted only a few percent of the sample.

On the basis of the profile analysis, it was also possible to individuate the presence of an additional diffraction component close to the spinel peaks in the $x > 0.35$ samples (9). As an example, the inset of Fig. 1 shows the different broadening of the diffraction profiles of the 444 reflection for $x = 0.35$ and $x = 0.37$ samples. The spinel peaks of the $x = 0.37$ sample can be fitted using two p-Voigt functions. The pair of fitting functions was always constituted by a sharp gaussian function at lower angle and a broad lorentzian function at a higher angle. The set of sharp gaussian peaks, corresponding to the larger spinel cell, refers to the stoichiometric one, while the set of broad lorentzian peaks represents the diffraction effects of the contracted nonstoichiometric spinel cell. Such a procedure makes it possible to distinguish between the two limiting spinel forms. The presence of a Li-rich spinel phase, in addition to the stoichiometric phase in the $x > 0.35$ samples, was taken into account in the successive Rietveld analysis. The stoichiometry of both phases is directly derived by the refinement of the occupancy factors, as previously shown in (9).

Moreover, an indirect suggestion of the presence of nonstoichiometric spinel phase comes from comparing the amount of the Li_2MnO_3 phase resulting from the XRD analysis with the phase amounts expected in the binary system $LiMn_2O_4$–Li_2MnO_3 (Figure 2A). The experimental values of Li_2MnO_3 percentage are indeed systematically lower than the calculated values (continuous line) for $x < 0.40$. Thus, three phases were included in the structural model for the Rietveld profile refinement and the results are summarized in Table 1.

On the other hand, the percentage of Li_2MnO_3 is remarkably higher than the calculated values for $x > 0.44$. We

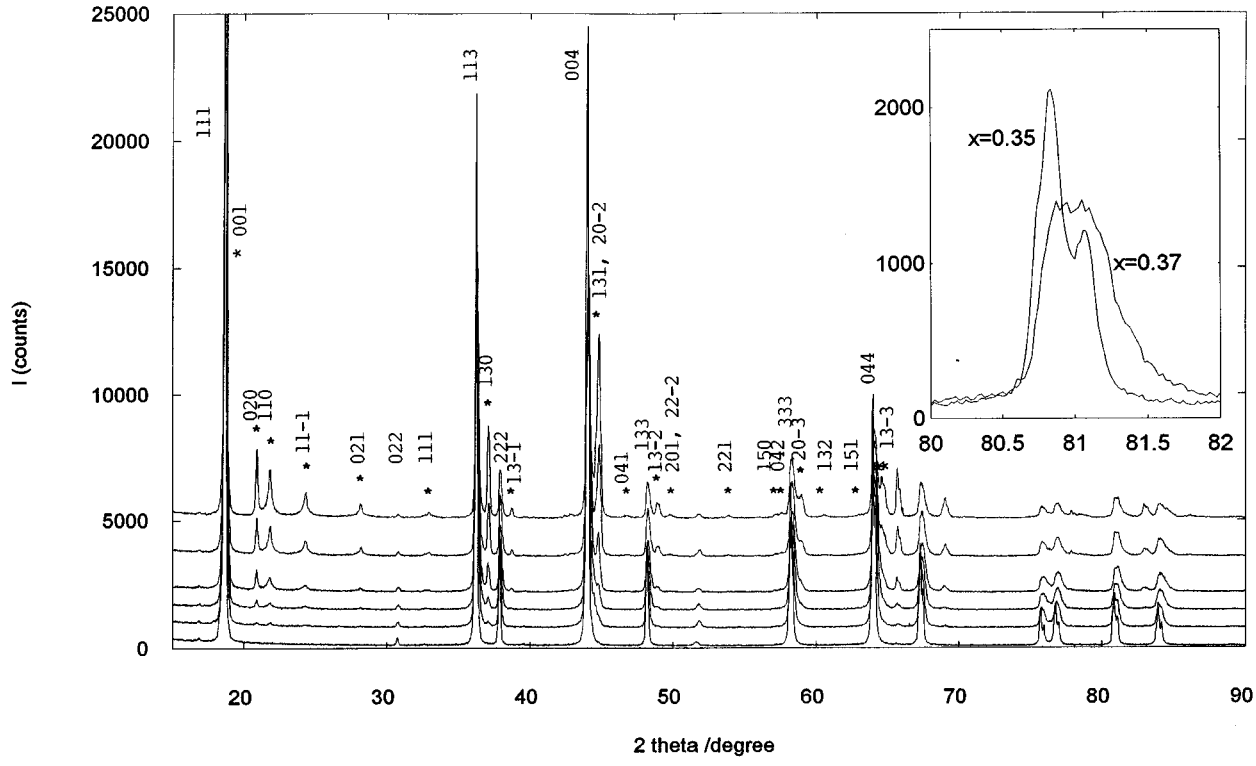

FIG. 1. X-ray powder patterns showing the appearance of the Li_2MnO_3 phase (Li_2MnO_3 peaks are marked by stars) with increasing x value: 0.35, 0.36, 0.37, 0.40, 0.42, and 0.47 (from the bottom). Miller indices of both cubic and monoclinic phases are reported; for the second phase only the indices of the strongest overlapped reflection are given. The inset shows the different broadenings of 444 diffraction peak observed in 0.35 and 0.37 samples.

observed a wide variety of peak profile shapes in the Li_2MnO_3 pattern. The peak shapes range between sharp gaussian and broad lorentzian function. The full width at half maximum (FWHM) of a large number of single peaks of the monoclinic Li_2MnO_3 phase are reported in Fig. 3 as a function of the diffraction angle. The Li_2MnO_3 data were compared with the FWHM angular dependence of the Pearson VII profile width (full line) obtained from the Rietveld refinement. We also evaluated the spread of the FWHM data by comparing with standard FWHM values, using a well annealed BaF_2 sample as a standard for the determination of the instrumental line broadening (9, 17). The measured FWHM values of BaF_2 and the pertinent parabolic interpolation (dashed curve) are also reported in Fig. 3 for comparison. It can be deduced that Li_2MnO_3 crystallite sizes are small and highly dependent on lattice directions. The spread should be due to the markedly anisotropic microstructure parameters (crystallite size and microstrain). An accurate investigation of such behavior is outside the aim of this work, but we supposed that this is the reason why the Rietveld profile fit gives increasingly worse discrepancy factors by increasing Li_2MnO_3 percentage. So the amount of this phase for $x > 0.44$, as well as the total lithium cationic fraction x_t, is probably overestimated (see Table 1).

It can be observed that both the lattice parameter values and the lithium content of the spinel phases are nearly independent of composition in the range $x > 0.36$. The only parameter showing large variation is the phase percentage. Such behavior is probably due to the sufficiently slow cooling process after the annealing, as described in Section 2.1.

Cases of coexistence of phases with the same structure but with different cation occupancies are quite frequent in the literature. For the lithium manganese spinel lattice parameter, values in the range $8.190 < a/\text{Å} < 8.247$ were obtained by several authors (4, 5, 16) using different synthesis conditions. The data in Table 1 show that the two coexisting spinel phases have different composition ($x = 0.33$ and $x \cong 0.40$) and quite different lattice parameter values (about 8.22 Å and about 8.20 Å respectively).

For what concerns pure Li_2MnO_3, our results evidenced very limited cationic disorder, according to the formula $[Li_{0.5}]_{(2c)}[Li_1]_{(4h)}[Li_{0.489(1)}Mn_{0.011(1)}]_{(2b)}[Mn_1]_{(4g)}O_3$. The compound is nearly stoichiometric with $x = 0.663(11)$. The profile refinement based on a model with substitutional defect (6% or more, not variable) was performed: an

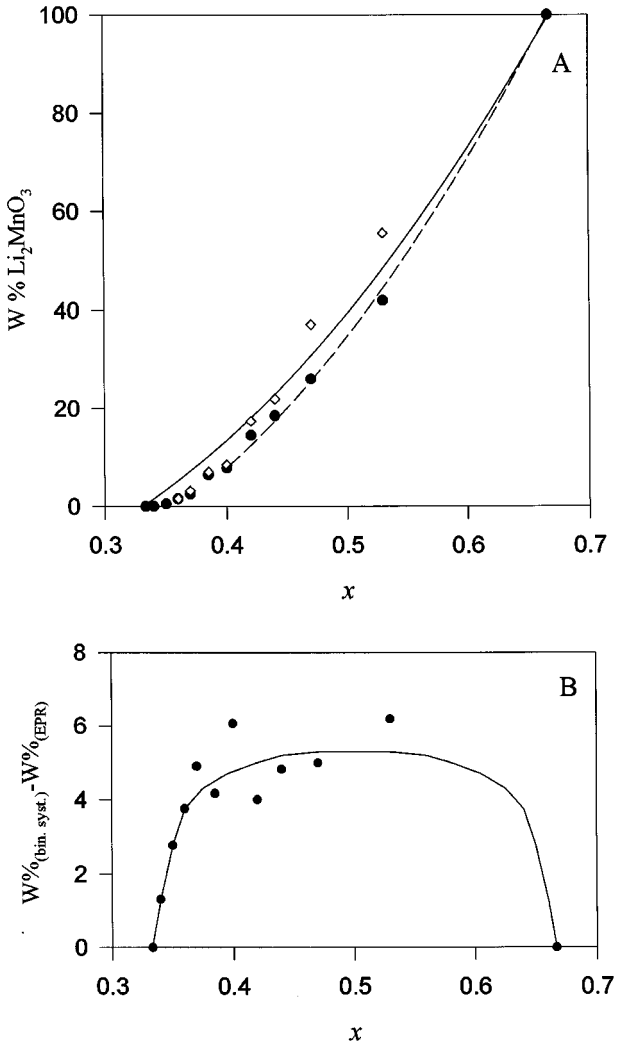

FIG. 2. (A) Quantitative EPR (●) and XRD (◇) Li_2MnO_3 weight% determinations compared with the theoretical curve of the x dependence of the phase in the binary mixture with stoichiometric spinel phase (full line). The calculated Li_2MnO_3 weight% in the ternary mixture $LiMn_2O_4$, $Li_{1+y}Mn_{2-y}O_4$ ($y = 0.21$), and Li_2MnO_3 (see text) is also reported (dashed line). (B) Difference between theoretical Li_2MnO_3 percentage, according to the binary mixture model, and EPR data as a function of x. The solid line is a guide to the eye.

increase of the discrepancy factor was observed by increasing the cation substitution. In addition, for variable site occupancies the initial cationic disorder decreased rapidly, giving the above formula again.

3.2. EPR Data

The EPR signal of our samples ($x \geq 0.33$) is composed, at room temperature, of a broad signal with linewidth $\Delta B \cong 300$ mT and g-factor $g \cong 2$ and a sharp line with $\Delta B = 21$ mT and $g = 1.994_5$ whose intensity increases with x. At 125 K the broad line disappears, after further broadening, while the sharp line remains practically unchanged. Figures 4c and 4d show the EPR spectra of the $x = 0.35$ sample at 293 and 125 K, respectively. We attribute the broad line to the spinel phase: it constitutes the only component of the EPR signal for $x = 0.33$ sample (Fig. 4a and 4b). No change was observed in the EPR signal ascribable to the Jahn–Teller transition recently reported (18) at 280 K.

On the other hand, the sharp signal is related to the presence of Li_2MnO_3 phase. A pure Li_2MnO_3 sample gives a very intense EPR signal, symmetric, with $g = 1.994_5$ and ΔB variable between 21 mT at 293 K and 25 mT at 125 K, as shown in Figs. 4e and 4f, respectively. Its shape is lorentzian and the area, compared with a standard, corresponds to a paramagnetic center density as high as $5 \times 10^{21}\ g^{-1}$ which also corresponds to the concentration of Mn^{4+} ions in the sample.

The EPR signal of Li_2MnO_3 is therefore a marker for the presence of such a phase. In fact, the same sharp signal is observed in all the $x > 0.33$ samples. Since its shape is the same in all the samples it is easy to determine the percentage of the phase from the simple ratio of the intensities, taking into account the masses of the samples, which may be very different to keep constant the Q-factor of the resonant cavity. This method allowed us to reach sensitivity for the presence of the phase down to 0.01%, at least. That was particularly useful for samples having composition in the range $0.33 < x \leq 0.35$, for which diffractometric measurements gave no response to traces of the Li_2MnO_3 phase. Moreover, the constant line shape in all the samples confirms that the Li_2MnO_3 phase remains separated and well distinguishable in the observed composition range. The quantitative EPR determinations are reported in Table 1 and in Fig. 2A (full circles) together with the XRD results and compared with the theoretical curves of the x dependence of Li_2MnO_3 wt% (see 3.1). The EPR results give systematic lower values with respect to those calculated from the binary system model and agree with the XRD data for $x \leq 0.4$.

The trend of the difference between calculated (binary system) and EPR Li_2MnO_3 percentage as a function of x (Fig. 2B) gives evidence of the x dependence of Li-rich spinel amount. This increases rapidly for $0.33 < x < 0.40$, does not actually change for $0.40 < x < 0.60$, and finally decreases for x increasing up to 0.667.

4. DISCUSSION

We now discuss the XRD and EPR results starting from the EPR signal that we found to be a peculiar marker of Li_2MnO_3 phase. The origin of this signal is indeed the Mn^{4+} ion (d^3 with $L = 3$ and $S = 3/2$) (19, 20). A ^4F ion in octahedral coordination, although characterized by some degree of distortion, possesses a singlet orbital Γ_2 ground state with spectroscopic factor $g = g_e - 8\lambda/\Delta < g_e$ and less

Table 1

x_{Li}	0.35	0.36	0.37	0.385	0.40	0.42	0.44	0.47	0.53	0.67
					Stoichiometric spinel					
R_B[a]	5.22	3.75	3.90	4.18	3.98	4.69	4.85	4.95	4.22	
a/Å	8.2296(1)	8.2282(1)	8.2258(1)	8.2253(1)	8.2223(1)	8.2264(1)	8.2252(1)	8.2275(1)	8.2304(1)	
% phase	100.00	49.35	41.23	40.96	40.17	49.36	46.85	35.31	24.55	
Formula	$Li_{1.06(2)}Mn_{1.94(2)}O_4$	$LiMn_2O_4$	$LiMn_2O_4$	$LiMn_2O_4$	$LiMn_2O_4$	$LiMn_2O_4$	$LiMn_2O_4$	$LiMn_2O_4$	$Li_{1.04(5)}Mn_{1.96(5)}O_4$	
					Nonstoichiometric spinel					
R_B[a]		3.59	3.22	3.88	2.66	3.39	2.73	2.72	5.30	
a/Å		8.2111(3)	8.2038(2)	8.2038(3)	8.1990(3)	8.1999(5)	8.2006(4)	8.2014(3)	8.2042(2)	
% phase		49.00	55.56	51.96	51.32	33.23	31.19	27.59	19.79	
Formula		$Li_{1.17(2)}Mn_{1.83(2)}O_4$	$Li_{1.14(2)}Mn_{1.86(2)}O_4$	$Li_{1.12(2)}Mn_{1.88(2)}O_4$	$Li_{1.19(2)}Mn_{1.81(2)}O_4$	$Li_{1.28(3)}Mn_{1.72(3)}O_4$	$Li_{1.27(3)}Mn_{1.73(3)}O_4$	$Li_{1.27(4)}Mn_{1.73(4)}O_4$	$Li_{1.22(5)}Mn_{1.78(5)}O_4$	
					Monoclinic Li_2MnO_3					
R_B[a]		22.85	15.91	14.41	12.55	10.64	11.36	10.33	10.83	6.89
a/Å		4.9189(5)	4.9273(2)	4.9238(2)	4.9241(1)	4.9242(1)	4.9228(1)	4.9236(1)	4.9238(1)	4.9245(1)
b/Å		8.5171(8)	8.5189(4)	8.5181(3)	8.5217(2)	8.5210(2)	8.5196(2)	8.5219(2)	8.5216(2)	8.5215(1)
c/Å		5.0730(6)	5.0381(3)	5.0283(2)	5.0272(1)	5.0260(1)	5.0253(1)	5.0252(1)	5.0247(1)	5.0244(1)
β/°		109.2403(70)	109.3511(32)	109.3584(21)	109.3375(15)	109.3479(14)	109.3513(14)	109.3503(12)	109.3633(13)	109.3983(8)
% phase		1.65	3.21	7.08	8.51	17.41	21.96	37.10	55.66	100
% phase EPR[b]	0.51	1.57	2.50	6.44	7.85	14.50	18.50	26.00	42.00	100
					Global parameters and factors					
R_p[c]	12.55	7.52	7.27	8.16	7.58	9.19	9.50	10.20	11.82	13.37
R_{wp}[d]	17.88	11.12	10.64	11.91	10.82	12.71	13.36	14.24	16.52	17.67
S[e]	3.11	2.15	2.07	2.41	2.15	2.54	2.50	2.79	3.13	3.54
x_t[f]	0.353	0.369	0.375	0.388	0.406	0.443	0.458	0.512	0.565	0.663

[a] Bragg discrepancy factor (see Ref. (12)).
[b] Li_2MnO_3 weight% deduced from EPR data.
[c] Profile discrepancy factor (see Ref. (12)).
[d] Weighted profile discrepancy factor (see Ref. (12)).
[e] Goodness of fit.
[f] Total lithium cationic fraction of the sample, calculated from abundance and Li content of each phase.

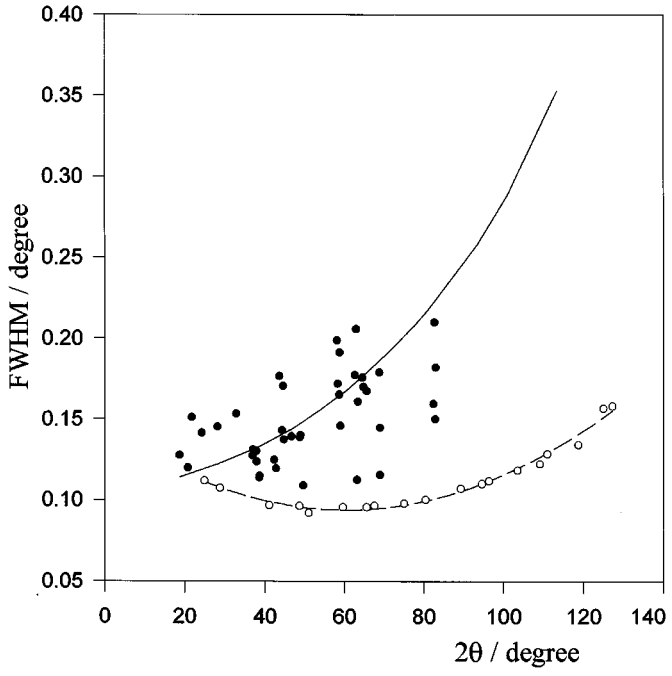

FIG. 3. Full width at half maximum dependence of the diffraction angle for Li_2MnO_3 (●) and BaF_2 standard (○) peaks, compared with: (full line) Pearson VII width from the Rietveld refinement; (dashed line) parabolic interpolation of BaF_2 data.

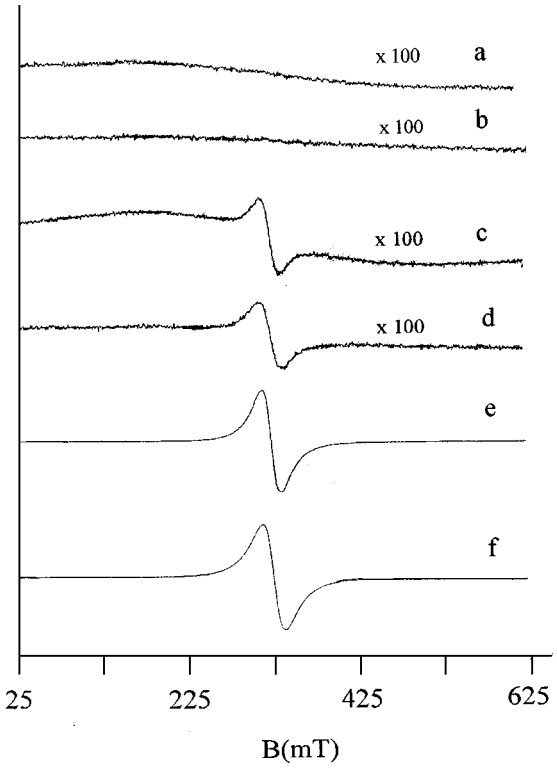

FIG. 4. EPR signal of the $x = 0.33$ sample (pure $LiMn_2O_4$) at 293 K (a) and 125 K (b), of the $x = 0.35$ sample at 293 K (c) and 125 K (d), and of the $x = 0.667$ (pure Li_2MnO_3) sample at 293 K (e) and 125 K (f). In (a) and (c) the broad EPR signal can be observed.

than 2 (21). Indeed, the oxygen octahedron around Mn^{4+} is strongly distorted, as can be evinced from the above structure data, but no feature due to anisotropy was observed from the powder signal shape. In fact, if the $S = 1/2$ state is the lowest in energy, the intensities of transitions involving the $S = 3/2$ spin state are quenched in a powder spectrum because of the strong angular dependence of the pertinent resonances and the signal is symmetric. It is interesting to note that, although this is not a "diluted" magnetic system, the observed ΔB value is small and nearly constant within the observed temperature range. Each Mn^{4+} ion has only three Mn^{4+} ions among its nearest neighbors: this makes the dipolar interactions lower while the superexchange interaction at 90° provides a consistent exchange narrowing of the signal. This effect is evidenced by the lorentzian lineshape and proved by the existence of antiferromagnetic order below 50 K (22).

The features of the broad EPR signal do not make it possible to discriminate between stoichiometric and nonstoichiometric spinel. However, on the basis of its calculated area, this signal can be attributed to Mn^{4+} ions or holes introduced by the lithium in the spinel phase, since the relative EPR center density seems to match the percentage variation with respect to the total Mn content of such an ion, ranging between 50% and 78% for $0.33 \leq x \leq 0.40$ (9).

The absence of exchange narrowing effects on the EPR signal in the spinel phase may have different origins. Assuming hole localization on Mn^{3+} ions, the resulting Mn^{4+} ions should be surrounded by nearly regular oxygen octahedra as for Mn^{3+}: the superexchange interactions between nearest neighbor Mn ions would take place only for 90° bond angles, since the tetrahedral sites are occupied by Li^+ ions. However, part of the Mn^{3+} ions may be in low spin configuration (23) or replaced by Li^+, making a simple prediction about exchange interactions unreliable. No recent information is available about the magnetic transition of the spinel phase, although magnetic susceptibility measurements (23) suggest antiferromagnetic behavior for $T < 100$ K. Moreover, double exchange phenomena due to electron hopping should not be excluded in cases of crystallographic equivalence of the Mn^{4+} and Mn^{3+} sites (24).

The EPR results of Li_2MnO_3 percentage give lower values with respect to the binary system model, as shown in Fig. 2. Such a result, pertinent to the whole x range, represents a further strengthening of the hypothesis of the presence of a Li-rich spinel phase in addition to the stoichiometric phase. The saturation of the difference curve of Fig. 2B allows one to estimate the maximum lithium excess in the Li-rich spinel phase, i.e. $Li_{1+y}Mn_{2-y}O_4$, with $y = (3x - 1) = 0.20$. This result is indeed very close to the XRD averaged value $y = 0.21(6)$ (see Table 1). The

experimental data for $x > 0.40$ can be interpreted on the basis of a model constituted by Li_2MnO_3 and two spinel phases in equal amounts but with different compositions: the stoichiometric and a nonstoichiometric phase with $y \cong 0.21$ (dashed line, Fig. 2A).

The present results make it possible to define both the range of nonstoichiometry of the spinel phase and the possible role of the anisotropy of Li_2MnO_3 microstructure parameters in causing XRD overestimation of its percentage. There is evidence that poor reliability of XRD Rietveld refinement results affects the determination of the effective occupancy of the lithium sites in the spinel structure. For most reliable use of quantitative Rietveld analysis of multiphase systems, extensive tests are needed over the complete composition range.

REFERENCES

1. P. Barboux, J. M. Tarascon, and F. K. Shokoohi, *J. Solid State Chem.* **94,** 185 (1991).
2. J. M. Tarascon, W. R. McKinnon, F. Coowar, T. N. Bowmer, G. Amatucci, and D. Guyomard, *J. Electrochem. Soc.* **141,** 1421 (1994).
3. J. C. Hunter, *J. Solid State Chem.* **39,** 142 (1981).
4. M. M. Thackeray, P. J. Johnson, L. A. de Picciotto, P. G. Bruce, and J. B. Goodenough, *Mater. Res. Bull.* **19,** 179 (1984).
5. G. Pistoia, G. Wang, and C. Wang, *Solid State Ionics* **58,** 285 (1992).
6. G. A. Martin, A. Bates, V. Ducarme, and C. Mirodatos, *Appl. Catal.* **47,** 289 (1989).
7. J. A. Price and O. K. Carlson, "Group I–A metal manganites, manganates and cobaltites as polyester polycondensation", Patent US-XXAM-US 3475380 691028—US670203.
8. K. R. Morgan, S. Collier, G. Burns, and K. Ooi, *J. Chem. Soc. Chem. Commun.* **2,** 1719 (1994).
9. V. Massarotti, M. Bini, and D. Capsoni, *Z. Naturforsch. A* **51,** 267 (1996).
10. P. Strobel and B. Lambert-Andron, *J. Solid State Chem.* **75,** 90 (1988).
11. H. M. Rietveld, *J. Appl. Crystallogr.* **2,** 65 (1969).
12. J. Schneider, *in* "Proceedings, IUCR International Workshop on the Rietveld Method, Petten, 1989".
13. D. B. Wiles and R. A. Young, *J. Appl. Crystallogr.* **14,** 149 (1981).
14. V. Massarotti, D. Capsoni, and M. Bini, *Z. Naturforsch, A* **50,** 155 (1995).
15. R. J. Hill and C. J. Howard, *J. Appl. Crystallogr.* **20,** 467 (1987).
16. D. G. Wickham and W. J. Croft, *J. Phys. Chem. Solids* **7,** 351 (1958).
17. J. I. Langford, NIST, Spec. Pub. **846,** p. 110, Gaithersburg, MD, 1992.
18. A. Yamada and M. Tanaka, *Mater. Res. Bull.* **30,** 715 (1995).
19. A. Scharmann, B. Vitt, R. Hoppe, and G. Meyer, *Phys. Status Solidi B* **72,** 197 (1975).
20. A. Hofstaetter, A. Scharmann, and B. Vitt, *Phys. Status Solidi B* **84,** 93 (1977).
21. A. Abragam and B. Bleaney, *in* "Electron Paramagnetic Resonance of Transition Ions", p. 430, Clarendon, Oxford, 1970.
22. M. Jansen and R. Hoppe, *Z. Anorg. Allg. Chem.* **397,** 279 (1973).
23. L. Shutte, G. Colsman, and B. Reuter, *J. Solid State Chem.* **27,** 227 (1979).
24. P. De Gennes, *Phys. Rev.* **118,** 141 (1960).